Properties of the triangular excitation pulse and the 3D heat transfer effects in the excitation pulse method

Rasooli, Arash; Itard, Laure

Important note
To cite this publication, please use the final published version (if applicable).
Please check the document version above.

Properties of the Triangular Excitation Pulse and the 3D Heat Transfer Effects in the Excitation Pulse Method

Arash Rasooli[1,], Laure Itard[1]*

[1]OTB: Research for the Built Environment, Delft University of Technology, Julianalaan 134, Delft, the Netherlands

Abstract. Concerning the high levels of energy consumption in the existing building stock, the necessity for characterization of the building envelop is a well-known issue. Accordingly, numerous methods and practices have been developed and studied to measure the thermal resistance and other thermal characteristics of the walls in-situ. In the current paper, a previously proposed method, the Excitation Pulse Method, EPM, based on the theory of thermal response factors, is further studied and investigated through simulations, to rapidly measure the thermal resistance of existing walls. A prototype is built and introduced to carry out larger number of measurements on site. The triangular pulse's properties such as the relation between its magnitude and its time interval on its corresponding response are investigated. It is shown how changes in time interval can make the method sensitive to the number of residuals and affect its reliability. General constraints and validity domain of the method are studied. In addition, the effect of 3D heat transfer on the performance of the method is further illustrated in light and heavy constructions. It is shown in which cases it is possible to apply the method in-situ and measure the thermal resistance within a couple of hours.

1 Introduction

The high levels of energy consumption in buildings as a result of heating demand requests special attention as it consequently gives also a huge potential for energy saving [1]. Accordingly, many studies have been dedicated to find out the most important parameters influencing buildings' thermal behavior and their energy demand [2-4]. Amongst various building components, exterior walls are responsible for a considerable rate of heat loss. Consequently, determination of their thermal properties through theoretical [5-7], in-lab [8, 9], and in-situ [10-15] methods have been given much devotion. In 2016, a transient in-situ method, Excitation Pulse Method (EPM) [16], based on the theory of Response Factors (RFs) was developed and tested on three case studies [17] as a proof of principle. The method has shown to potentially aid in a reliable rapid measurement of walls' thermal resistance (R_c-value), within a couple of hours. As a potential was observed in the performance of the method, the research was continued to further test and validate it to elevate its performance for further measurements. In this paper, new details regarding the application of the method are presented. A prototype is built and shown to further test the method in more samples in-situ and in the lab.

1.1 EPM and the theory of RFs

EPM is based on the theory of RFs. The same excitation pulse (linear heating followed by linear cooling and keeping the surface temperature at the initial level) as

described in the theory of the method [18] is applied to the surface of the wall using a heater and a cooling unit. The two heat flux responses at two sides are measured via heat flux meters and the surface temperatures are measured via high accuracy thermocouples and controlled accordingly. The exterior surface of the wall is protected via a reflective semi-insulating cover to minimize the effects of outdoor heat flux disturbances on the measurement of the heat fluxes. In **Fig. 1**, the general concept of the method and its equipment are shown.
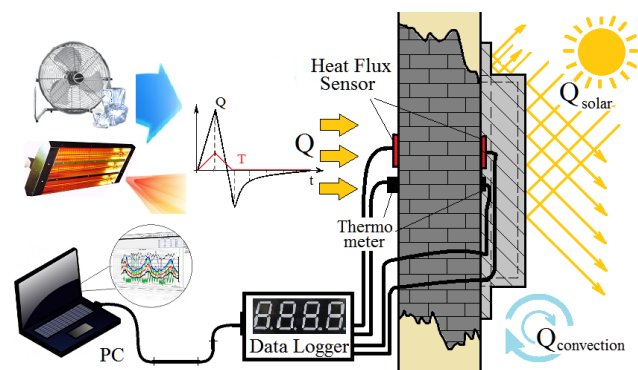

Fig. 1. The EPM and its equipment: applying a triangular temperature pulse to the surface of the wall via heater and cooler and measuring the heat flux responses at both sides

As the RF theory is based on Laplace transform and therefore superposition is allowed, in order to overcome the noise in the temperature and the heat flux, the pulse is applied at a magnitude (δ) much higher than 1 K (as the RF theory prescribes). This way, the disturbances

---
[*] Corresponding author: A.Rasooli@tudelft.nl

from heat flux and temperature become negligible. The consequent heat flux responses $\dot{q}$ at sides 1 (excitation side) and 2 (opposite side) are therefore, divided by the magnitude of the pulse to obtain the RFs (X_i at side 1 and Y_i at side 2) as follows:

$$\begin{cases} X_i = (\dot{q}_1)_i / \delta \\ Y_i = (\dot{q}_2)_i / \delta \end{cases} \tag{1}$$

Where, the subscript i is the RFs' index. From the calculated RFs, the walls' main thermo-physical characteristics such as the R_c-value can be obtained based on both [16] in (2), or either of the surfaces in (3):

$$R_c = 2 \times \left(\sum_{i=0}^{N} (X_i + Y_i) \right)^{-1} \tag{2}$$

$$R_c = \frac{1}{\displaystyle\sum_{i=0}^{N} X_i} = \frac{1}{\displaystyle\sum_{i=0}^{N} Y_i} \tag{3}$$

For a light wall, as it is usually possible to obtain the Y factors easily, the use of (2) is beneficial as it results in a quicker obtaining of the R_c-value [16]. For the heavily-constructed (high thermal mass) and highly insulated (high R_c-value) walls, as it is usually difficult to observe a significant rise in the exterior heat flux, it is better to use (3) for the X RFs. As for some constructions it may take several hours for the X RFs to reach the end of the time-series X (time axis), it is possible to measure few of RFs and as use the constant ratio [19], to estimate the rest based on the ratio and the last measured RF.

2 Building the Prototype

As the method has shown to require a certain level of preciseness for the execution and the control [16], it is not appropriate to perform it manually. Consequently, a prototype is built to apply the triangular excitation pulse and control the desired surface temperature profile. While previously the variable heat flow was adjusted by moving the radiative heater, the prototype executes this step by continuous adjustment of heat flux through variable power, via a dimmer. Following the linear heating, linear cooling consists of four stages (**Fig. 2**):

1. Dimming down the heating
2. Heat removal via natural convection (no fan)
3. Heat removal via forced convection (fan)
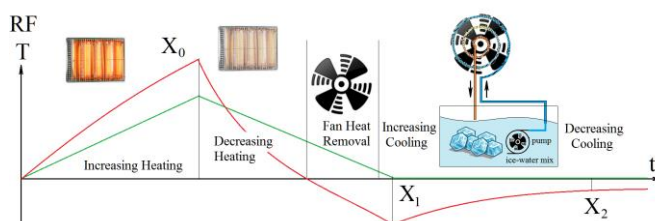4. Heat removal via forced convection (fan and coil)

Fig. 2. Heating and cooling stages in EPM: The triangular pulse is generated using a heater and a cooling system.

In the prototype, a fan, cooling water, and ice bricks are integrated into one cooling system. The fan has been equipped with a spiral tube in which cool water is circulated by a pump. Ice bricks are placed in the water container to keep the temperature at 0 C. The fan applies a forced convection to the wall over the tube, decreasing the air flow temperature significantly. In **Fig. 3**, the schematic view of the system (on the right) and its actual photos (on the left) are shown.
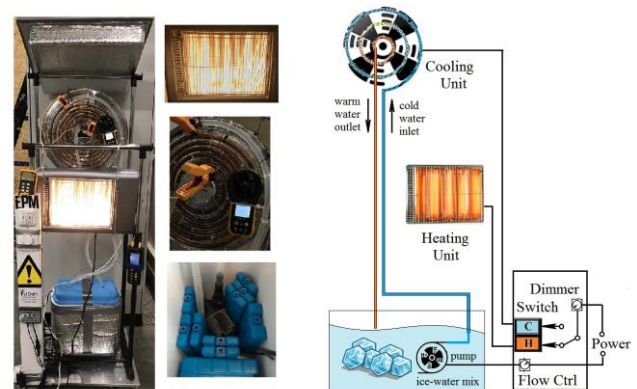

Fig. 3. Schematic view (right) and the actual photo (left) of the EPM prototype and its components

The built prototype has been used and tested to carry out more measurements in a lab. The results of these experiments and their post processing will be presented in 2019.

3 Heat Transfer Simulations and Results

Simulations of heat transfer based on finite element method have been carried out in COMSOL Multiphysics 5.3a [20] to study various possibilities for performing measurements. The simulations have been made in such a way that they represent actual experiments (inspired by experience and measured data) as much as possible. Boundary conditions include surface temperature of 293 K) for indoor side and 288 K for outdoor side of the wall. The initial condition is an average temperature of 285.5 K for the solid domain. The indoor surface of the wall is given a pulse of δ K above the indoor surface temperature, after it has reached a quasi-steady state (as it is supposed to be during the experiment). The heat fluxes at indoor and outdoor sides are computed at the center and the opposite side of the heated area (where in the real measurements the heat flux sensors and thermocouples are mounted).

3.1. Time Interval vs Pulse Magnitude

As the feasibility of EPM includes a non-destructive approach, it is of great importance to prevent damage to the finishing of the indoor wall (e.g. wallpapers). Accordingly, if the surface is sensitive to the heat and high temperature, it is required to apply a pulse of a lower magnitude. To ensure that the heat imposed to the wall is of enough quantity, the base of the triangle

should increase when the height decreases. This way, equal amounts of heat can be applied to the surface. In **Table 1** and **Fig 4**, the results of three experiment simulations of a 0.2 m brick wall are presented. Three pulse magnitudes of 80 K, 40 K, and 20 K are combined with time intervals of 20 min, 40 min, and 80 min respectively. The X_0, being the first RF, derived from the peak of the heat flux decreases as the time interval becomes larger. R_c^{th} is the theoretical R_c-value, based on construction, R_c^{EPM} is the R_c-value resulted from an EPM simulation and calculated by (3).

Table 1. Combination of time intervals and pulse magnitudes modelled for a brick wall and the resulted R_c-value

t [min]	δ [K]	X_0 [Wm^{-2}K^{-1}]	R_c^{EPM} [m^{2}KW^{-1}]	R_c^{th} [m^{2}KW^{-1}]
20	80	26	0.24	0.24
40	40	19	0.25	0.24
80	20	13	0.25	0.24

The results of RFs generated by the various time intervals and pulse magnitudes are presented in **Fig. 4**.
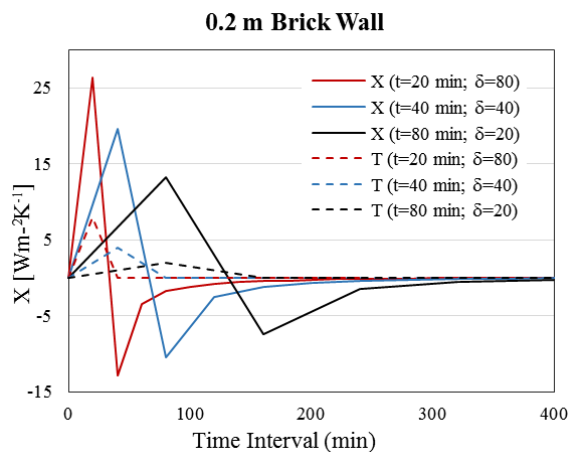

Fig. 4. Combination of various pulse magnitudes and time intervals in 0.2 m brick wall

As seen in **Fig. 4**, different time intervals can be combined and applied with different pulse magnitudes. The selectivity of different combinations allows higher flexibility and therefore higher efficiency in measuring components of various sizes and constructions. For instance, in a heavy construction, in order to ensure sufficient heat penetration, a larger magnitude with a longer time interval can be used. Note that in these cases, the heated area should be as large as possible and the measurement takes place at the center of the heated area.

3.2. Time Interval vs number of RFs

As observed in **Fig. 4**, the number of RFs (N in (2) and (3)) also changes as the time interval varies. The total time required for the wall to absorb and conduct the heat from the excitation pulse determines N. The total time is a function of thermal response time [21] which depends on the construction. The required number of RFs

(defined as the minimum number of RFs needed in (2) or (3) to find an accurate R_c-value) increases as the time interval of the RFs becomes shorter. The required number of the RFs with an index greater than 3, as well as the dependence of the R_c-value to these RFs increases consequently. In **Fig. 5**, the results of the post processing of a simulation of a brick wall (*thermal conductivity* 0.9 Wm^{-1}K^{-1}, density 2000 kgm^{-3} and specific heat capacity 840 Jkg^{-1}K^{-1}) are shown. The dashed curves show how the minimum required number of RFs (*N required*) decreases in different thicknesses as a longer time interval is chosen. Note that in EPM, not all the RFs are measured since using (2) shortens the measurement time significantly. Additionally, RFs with indices higher than 3 can be estimated rather than measured when (1) is used.
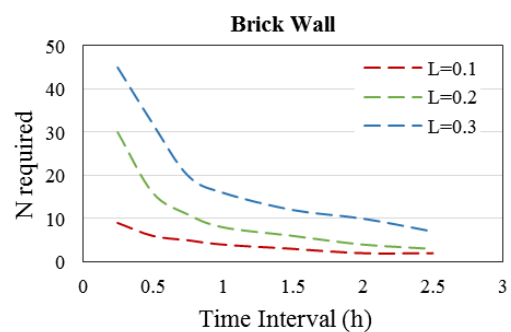

Fig. 5. Minimum required number of RFs vs time interval for a brick wall in different thicknesses *L*

The necessity of having a minimum number of RFs is based on the fact that if a lower number is used, the R_c-value is not accurate. This happens due to the fact that in such case, the *X* curve does not reach zero if *N* is smaller than the minimum required number of RFs. In **Fig. 6**, the R_c-value is calculated via (1), with the required number of RFs (*N required*) in black dashed line, being accurate enough and therefore in-line with the actual R_c-value (dotted red line). The same procedure is repeated also for only 4 RFs (*N required* for the time interval of 2h), resulting in a higher difference (solid black line) when a shorter time interval is chosen. The blue dashed-dotted line shows the error in finding the R_c-value from (1) if only 4 RFs (*N* for the time interval of 2h) are used.
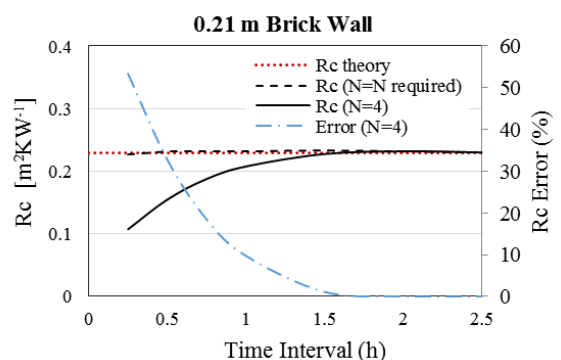

Fig. 6. Sensitivity of the R_c-value to the number of RFs in a 21 cm brick wall

3.1. Dealing with 3D heat transfer effects

Since the heat pulse is applied only to a certain area of the wall, depending on the size of the heater, the risk of three-dimensional heat transfer exists. Especially, due to the fact that the temperature gradient between the heated domain and the non-heated domain is high, chances are that the heat flux in the directions of width (q_x) and height (q_z) of the wall become considerable and even comparable to the one in the direction of the thickness (q_y). This issue is negligible in thin walls and becomes more important in thick walls. The heat transfer in any direction has the following rate:

$$\dot{q}_{x,y,z} = (\frac{1}{R_{x,y,z}})\Delta T_{x,y,z} \qquad (4)$$

Two parameters, the first one being the thermal resistance R and the second one being the temperature gradient contribute at the same time to the 3D heat transfer effects and in this case in the measurements carried out using EPM.

On the one hand, the whole body of the wall can be considered as a system (**Fig. 7**) of resistors (and capacitors) which can be divided into separate parts in lateral directions. The middle part (where the heating is applied in y direction) can be modelled as a control volume with same resistances (R_y) in all directions, bounded by much larger resistances in height (R_z) and width (R_x) direction.
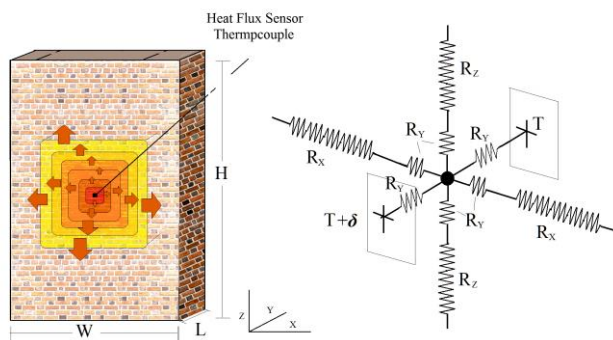

Fig. 7. The 3D heat transfer effect due to the resistance network: the wall modelled as a network of resistances

The resistances in different directions can be calculated as follows:

$$\begin{cases} R_y = \int_0^{L/2} k\,dy = L/2k \\ R_x = \int_0^{(W-L)/2} k\,dx = (W-L)/2k \\ R_z = \int_0^{(H-L)/2} k\,dz = (H-L)/2k \\ H, W \gg L \end{cases} \qquad (5)$$

Where R is the thermal resistance, and x, y, and z are space coordinates, and k is thermal conductivity. Since in a wall the height H and the width W of a wall are much

larger than its thickness L, R_x and R_z are considerably greater than R_y. As the height and width directions include these additional large resistances, in normal conditions and constant temperature gradient ΔT in the whole domain, the heat $\dot{q}$ in the center line direction (y axis) has a higher tendency to flow towards the smaller resistance (R_y) and not towards the much larger lateral ones (R_y+R_z and R_y+R_x):

$$\begin{cases} \dfrac{\Delta T}{R_x} \ll \dfrac{\Delta T}{R_y} \rightarrow \dot{q}_x \ll \dot{q}_y \\ \dfrac{\Delta T}{R_z} \ll \dfrac{\Delta T}{R_y} \rightarrow \dot{q}_z \ll \dot{q}_y \end{cases} \qquad (6)$$

Obviously, this matter becomes more important as the thickness L and consequently the resistance R_y increase.

On the other hand, the temperature gradient is the driving force. When a large area is heated, the heat in the center has lower tendency to flow towards lateral directions because the lateral neighbor domains are also heated and therefore have a closer temperature (T^1_{High}) to the center (T_{High}). Accordingly, as the distance from the center is decreased, the heat will have a higher tendency to flow towards the depth direction, rather than the lateral directions. In **Fig. 8**, this concept is depicted.
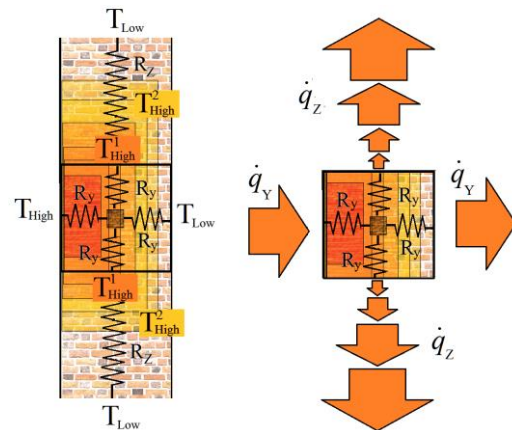

Fig. 8. 3D heat transfer effect due to the temperature gradient

The heat flows in different directions can be estimated as follows:

$$\begin{cases} T^1_{High} < T^2_{High} \ll T_{Low} \\ \dot{q}_y = (T_{High} - T_{Low})/R_y \\ \dot{q}_x = (T^1_{High} - T^2_{High})/R_x \rightarrow \dot{q}_x \ll \dot{q}_y \\ \dot{q}_z = (T^1_{High} - T^2_{High})/R_z \rightarrow \dot{q}_z \ll \dot{q}_y \end{cases} \qquad (7)$$

T is the temperature of each domain. T^1_{High} is greater than T^2_{High} and the difference becomes greater as the distance from the central line increases. Accordingly, again in (6), q_x and q_z are much larger than q_y. This

aspect is directly affected by the area where the heat is applied and therefore, requires considerations.

In **Fig. 9**, a 0.3m concrete wall is modelled. EPM is applied to this wall at the center in a diameter of 1.2m and the R_c-value can be obtained using (1). The heat flow in y direction (towards the thickness) in shown in solid black. The heat flows in z direction (towards the height) are shown in dashed lines. These values are much lower as the distance to the center line decreases.
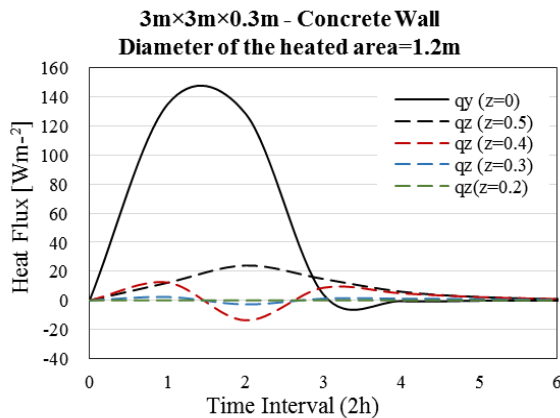

Fig. 9. Heat flux in z direction (dashed) in different distances from the y axis passing the center of the heated area in EPM and the heat flux in y direction (in solid black) at the same axis

Accordingly, in EPM it is always recommended to apply the pulse to an as large as possible area and measure the parameters only in the center of this area. This becomes more important when dealing with heavier walls.

In **Fig. 10**, a concrete wall of height H=3 m and width W=3 m is modelled in different thicknesses of L= 0.1 m, 0.21 m, 0.35 m, and 0.5 m. The diameter of the heated area is varied by different ratios of the width.
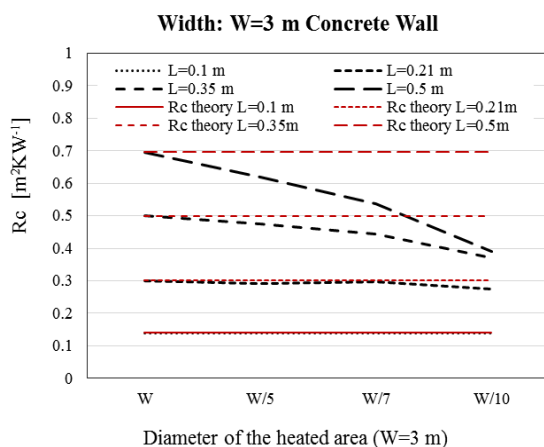

Fig. 10. Relation between the diameter of the heated area in EPM and the accuracy of the R_c-value measurement through EPM in different thicknesses of a 3×3 m^2 concrete wall

In addition to what was discussed so far, as long as the duration of the test is shorter than the thermal response time in lateral directions, the heat will flow towards the thickness direction before flowing in lateral layers and the measurement ends before the 3D heat transfer starts to affect it.

4. Conclusion

Further details of a rapid in-situ transient method, EPM, were introduced to apply it in large scale and a variety of constructions. The new control system has shown a more user-friendly application and the new cooling system has shown to be promising. Further experiments by this prototype will be shown in the near future. The RFs' time interval is investigated to show the possibility of combining various time intervals with different pulse magnitudes, allowing further flexibility and higher efficiency. As the number of RFs greater than 3 decreases with a higher time interval, the longer time interval is a better alternative as the residuals are difficult to record due to their small values. Additionally, the number of RFs shows to play an important role in the sensitivity of the results to the number of RFs. As demonstrated during the comparison of various pulse magnitudes and time intervals, it is concluded that for heavy constructions, a combination of largest possible signal and the longest possible time interval is better to be used. The analysis of the three-dimensional heat transfer effects showed a low tendency of the heat to transfer in lateral directions in light homogeneous walls. The effect of 3D heat transfer is generally rather limited except in very heavy constructions, resulting in a general advice regarding the size of the heated area. For heavy homogeneous walls, it is recommended to heat an as large as possible area and measure the parameters in the center of this area in order to minimize the lateral heat transfer risk. In the light homogeneous constructions however, this is not the case. More research will be done in the future, regarding the application and performance of the method, especially in multi-layered constructions.

References

1. Filippidou, F., N. Nieboer, and H. Visscher, *Effectiveness of energy renovations: a reassessment based on actual consumption savings.* Energy Efficiency: p. 1-17.
2. Ioannou, A. and L. Itard, *Energy performance and comfort in residential buildings: Sensitivity for building parameters and occupancy.* Energy and Buildings, 2015. **92**: p. 216-233.
3. Majcen, D., L. Itard, and H. Visscher, *Actual and theoretical gas consumption in Dutch dwellings: What causes the differences?* Energy Policy, 2013. **61**: p. 460-471.
4. van den Brom, P., A. Meijer, and H. Visscher, *Performance gaps in energy consumption: household groups and building characteristics.*

Building Research & Information, 2018. **46**(1): p. 54-70.

5. Deconinck, A.-H. and S. Roels, *Is stochastic grey-box modelling suited for physical properties estimation of building components from on-site measurements?* Journal of Building Physics, 2017. **40**(5): p. 444-471.

6. ISO, B., *6946: 2007 Building components and building elements—Thermal resistance and thermal transmittance—Calculation method*. 1923, British Board of Agrément tel.

7. Deconinck, A.-H. and S. Roels, *Comparison of characterisation methods determining the thermal resistance of building components from onsite measurements*. Energy and Buildings, 2016. **130**: p. 309-320.

8. Sala, J.M., A. Urresti, K. Martín, I. Flores, and A. Apaolaza, *Static and dynamic thermal characterisation of a hollow brick wall: Tests and numerical analysis*. Energy and Buildings, 2008. **40**(8): p. 1513-1520.

9. Martín, K., I. Flores, C. Escudero, A. Apaolaza, and J.M. Sala, *Methodology for the calculation of response factors through experimental tests and validation with simulation*. Energy and Buildings, 2010. **42**(4): p. 461-467.

10. ASTM, C., *1046-95 (Reapproved 2001): Standard practice for in-situ measurement of heat flux and temperature on building envelope components*. Annual Book of ASTM Standards, 2001. **4**.

11. ASTM, C., *1155-95 (Reapproved 2001): Standard practice for determining thermal resistance of building envelope components from the in-situ data*. Annual Book of ASTM Standards, 2001. **4**.

12. ISO, I., *9869: Thermal insulation—Building elements—In-situ measurements of thermal resistance and thermal transmittance*. International Organization for Standardization, Geneva, 2014.

13. Ahmad, A., M. Maslehuddin, and L.M. Al-Hadhrami, *In situ measurement of thermal transmittance and thermal resistance of hollow reinforced precast concrete walls*. Energy and Buildings, 2014. **84**: p. 132-141.

14. Rasooli, A. and L. Itard, *In-situ characterization of walls' thermal resistance: An extension to the ISO 9869 standard method*. Energy and Buildings, 2018. **179**: p. 374-383.

15. Flood, C., L. Scott, and C. Architects, *In Situ Thermal Transmittance of Case Studies in Dublin*. 2016.

16. Rasooli, A., L. Itard, and C.I. Ferreira, *A response factor-based method for the rapid in-situ determination of wall's thermal resistance in existing buildings*. Energy and Buildings, 2016. **119**: p. 51-61.

17. Rasooli, A., L. Itard, and C.I. Ferreira, *Rapid, transient, in-situ determination of wall's thermal transmittance*. REHVA European HVAC Journal, 2016. **53**: p. 16-20.

18. G. Mitalas, D.G.S., *Room thermal response factors*. ASHRAE Transactions, 1967. **73 (1) (1967)**: p. 1-10.

19. Kossecka, E. and J. Kosny, *Three-dimensional conduction z-transfer function coefficients determined from the response factors*. Energy and Buildings, 2005. **37**(4): p. 301-310.

20. COMSOL Multiphysics® v. 5.3.a www.comsol.com. COMSOL AB, S., Sweden.

21. Stewart, D.B., *Time-domain transient thermal response of structural elements*. Building and Environment, 1981. **16**(2): p. 87-91.